Postponed Air Entrainment in Dilute Suspension Coatings

Masato Yamamura, Hidenobu Miura, and Hiroyuki Kage
Dept. of Applied Chemistry, Kyushu Institute of Technology, Fukuoka, 8048550, Japan

DOI 10.1002/aic.10575
Published online May 27, 2005 in Wiley InterScience (www.interscience.wiley.com).

Experimental evidence is provided that the introduction of solid spheres significantly postpones the onset of air entrainment in a particular range of solid concentrations. Spherical poly(methylmethacrylate) particles were dispersed in Newtonian liquids at different weight fractions up to 1 wt %. Despite the monotonic increase in bulk liquid viscosity, the measured onset velocity of air entrainment first increased and then decreased with increasing particle number density. The maximum onset velocity was obtained at a certain particle number density that did not depend on either the particle diameter or the Bond number. A lubrication model was built by newly considering the forced air-film splitting by particle contacts. The successive consistency between the model prediction and the experimental observation suggests some directions for broadening the applicability of the coating operation to higher surface speeds. © 2005 American Institute of Chemical Engineers *AIChE J,* 51: 2171–2177, 2005
Keywords: air entrainment, suspension coating, dynamic wetting failure, film splitting, lubrication theory

Introduction

Forced wetting processes, in which gas at a moving solid surface is replaced by a liquid, are often accompanied by air intrusion between the liquid and the moving surface. Indeed, a direct observation using the laser-Doppler velocimetry revealed the existence of a thin air sheet in the order of 100 microns in length being retained downstream from the apparent contact line.[1] Two forces can compete in the continuous air film: the viscous lubrication force and the conjoining force that arises from attractive intermolecular forces. The former thickens the air film, whereas the latter tends to thin it. The resulting subtle balance of these forces generally reveals four flow regimes in its response to displacement speed. At low surface speeds (Regime I), the conjoining pressure can overcome the lubrication pressure. The Rayleigh–Taylor or Kelvin–Helmholtz instability can rupture the air film into fine bubbles,[2] leaving the residual air film only at a short distance beyond the apparent contact line. In Regime II at higher surface speeds, the air film is stabilized as a result of the stronger lubrication pressure. The liquid intersects the surface to form a straight contact line perpendicular to the moving direction (Figure 1a). With a further increase in surface speeds (Regime III, Figure 1b), the dynamic contact line spontaneously breaks into two or more inclined but still steady straight-line segments.[3] Increasing speeds even further (Regime IV, Figure 1c) leads to a regime in which subsequent cusp formation arising from a three-dimensional flow instability promotes an intermittent entrainment of visible air bubbles from downstream vertices of the inclined contact line segments.[4-6]

For "homogeneous" fluids involving no specific microstructures, extensive studies have focused on transitions between the flow regimes. Teletzke et al.[7] predicted the transition velocity between Regime I and Regime II by coupling a unidirectional lubrication flow equation with the conjoining pressure term. No continuous air film can be deposited in equilibrium below the critical displacement speed because the viscocapillary pressure is too low to prevent conjoining collapse. For a subsequent transition from Regime II to Regime III, Blake and Ruschak[3] demonstrated that the velocity component normal to the contact

Correspondence concerning this article should be addressed to M. Yamamura at yama@che.kyutech.ac.j.

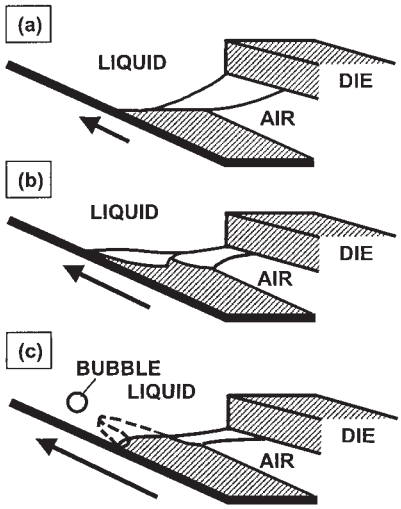

Figure 1. Perspective views of dynamic contact line with increasing substrate velocity.

(a) Regime II, (b) Regime III, (c) Regime IV.

line remains constant for a given fluid. They claimed that the molecular displacement by the adsorption/desorption process does not exceed a certain limiting velocity at the contact line. The existence of such a characteristic velocity was verified both in the angled coating experiments[8,9] and in the molecular displacement theory.[10] The last but the most drastic transition from Regime III to Regime IV occurs at a particular onset velocity of air entrainment, V_{ae}. An increase in bulk fluid viscosity generally results in the transition at a lower speed because of the stronger shear stress. For Newtonian fluids on a smooth surface, the onset velocity obeys the simple power law $V_{ae} \cong \mu^{-0.67}$, where μ is the bulk fluid viscosity.[4,11] From a practical perspective, a higher onset velocity of air entrainment is preferred to eliminate undesirable bubble and/or pinhole defects because the air entrainment often limits the operating speed and thus reduces the coating productivity.

However, the air film instability in a rigid "filler" suspension is still poorly understood. The introduction of solid additives in liquids is capable of disrupting the balance of the competing forces and thus changing the transition in flow regimes. In general, the flow around a filler promotes a viscous energy dissipation to increase bulk liquid viscosity. Classical hydrodynamic theories show that, at very low solid concentrations such that the flow around one filler is not influenced by the presence of neighboring fillers, the suspension viscosity is expressed by a simple linearly increasing function with respect to the solid volume fraction. Thus one would expect that the transition velocity between Regime III and Regime IV monotonically decreases with increasing filler concentration because of the resultant increase in liquid viscosity. In this article, we demonstrate evidence of a novel air entrainment behavior in which the introduction of insoluble solid spheres significantly increases the transition velocity in dilute suspensions. The onset velocity of air entrainment in the suspension was compared with that in the filler-free fluid to directly access the filler-induced air entrainment. The experimental results revealed that the instability through a free-surface cusp in the suspension is no longer considered a bulk phenomenon but rather involves interfacial contributions of each filler component.

Experimental Apparatus and Procedures

The experimental setup is schematically shown in Figure 2. The acrylic coating die filled with a test liquid was located on a rotating roller to feed the liquid. The steel roller (diameter: 300 mm; width: 300 mm) was driven by AC geared motors with a combination of timing pulleys and belts. The roller surface was mirror-finished. The coating gap, in which the liquid meniscus bridges the roller surface and the die edge, was set by placing shims between the roller and the bottom surface of the edge plate. Copper squeegees were pressed against the surface to remove the excessive liquid from the roll and to keep the surface as dry as possible. The liquids scraped off by the blade were caught in a pan located beneath the roll. The test fluids used were silicone oils (KF, Shin-Etsu Chemical) with different viscosities (μ_0) ranging between 0.054 and 0.31 Pa·s and surface tensions (σ) of 0.0208–0.0211 N/m. The viscosities of the filler-free liquids and suspensions were measured with a viscometer (Tokyo-Keiki Type BL) equipped with Couette geometry. The spherical poly(methylmethacrylate) particles (MBX, Sekisui Plastics) were dispersed in the coating liquids at different weight fractions up to 1 wt %. The particle diameter D_p ranged from 8 to 50 μm with a standard deviation of $<30\%$. The particles can settle by gravity at a finite time because of the density difference between the solid and the liquid. However, the downward particle motion by gravity was sufficiently slow compared to its transverse motion along the moving surface, that is, the terminal velocity of the particle was in the order of 10^4 lower than the roll speed. The dynamic wetting failure was visualized through the transparent edge plate of the die. The direct observation of the contact line allows us to measure the onset velocity of air entrainment corresponding to the transition velocity from Regime III to Regime IV. Stable dynamic contact lines were observed at relatively low roll speeds. With increasing roll speeds, visible air bubbles subsequently began to break off the trailing vertex. The roll speed, above which streaks of fine air bubbles were observed by the naked eye in the spreading liquid film, was defined as the onset velocity of air entrainment.

Results and Discussion

The major interesting features of the wetting failure in suspensions were the morphological changes in contact lines and

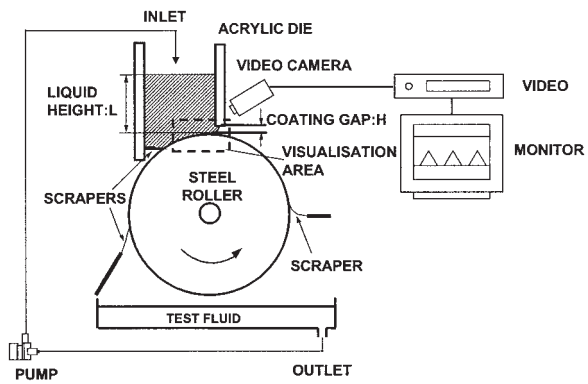

Figure 2. Experimental arrangement.

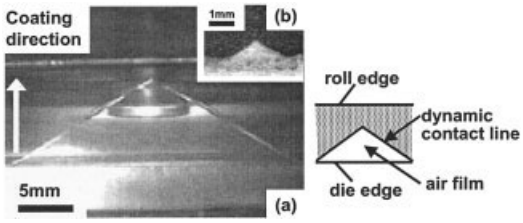

Figure 3. Snapshots of the dynamic contact lines at the onset of air entrainment.

(a) Filler-free fluid, (b) suspension case of $C_p = 0.1$ wt %. The roll surface moves from bottom to top as indicated by the arrow. The sawtooth pattern was significantly reduced in size in suspensions. The viscosity and the surface tension of the liquid were $\mu_0 = 0.116$ Pa·s and $\sigma = 0.0209$ N/m. The coating gap and the liquid height were $H = 50$ μm and $L = 6 \times 10^{-2}$ m.

the resultant variation in onset velocity of air entrainment. Figure 3 shows snapshots of the dynamic contact lines at the onset of air entrainment. The roll surface moves from bottom to top as indicated by the arrow. The viscosity and the surface tension of the liquid were $\mu_0 = 0.116$ Pa·s and $\sigma = 0.0209$ N/m, respectively. In the case of filler-free liquid (Figure 3a), the contact line adopted a sharp sawtooth configuration. The trailing vertex of inclined straight-line segments was located 7 mm downstream from the apparent contact line. The measured onset velocity of air entrainment (v_{ae0}) was found to be 0.176 m/s, showing good agreement with the predicted onset velocity from the power law.[11] On the contrary, the sawtooth pattern was significantly reduced in size in suspensions (Figure 3b). The resulting onset velocity of air entrainment increased to $v_{ae} = 0.337$ m/s, showing that an introduction of solid fillers can postpone the onset of wetting failure to higher surface speeds.

We next demonstrated how the suspension characteristics affect the dynamic wetting failure. Figure 4 shows the variation in onset velocity of air entrainment with the particle diameter. To quantify the postponed wetting failure in suspensions, the measured onset velocity was normalized as $(v_{ae} - v_{ae0})/v_{ae0}$,

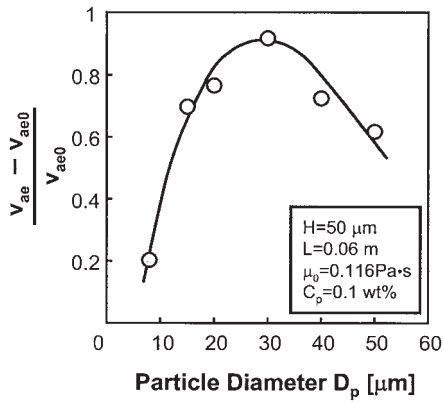

Figure 4. Variation in onset velocity of air entrainment with particle diameter.

The measured onset velocity was normalized as $(v_{ae} - v_{ae0})/v_{ae0}$, where v_{ae} and v_{ae0} are the onset velocities in suspension and filler-free fluid, respectively. The onset velocity reaches a peak at the particle diameter of 30 μm. The viscosity and the surface tension of the liquid were $\mu_0 = 0.116$ Pa·s and $\sigma = 0.0209$ N/m.

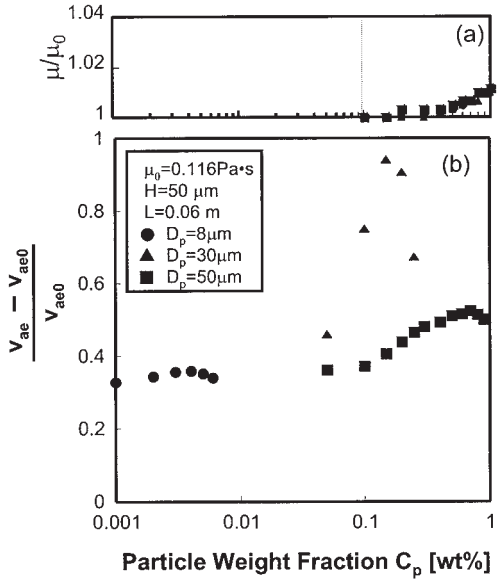

Figure 5. Variations in onset velocity of air entrainment and bulk suspension viscosity with particle weight fractions.

The measured suspension viscosity (μ) agreed with that of the filler-free liquid (μ_0) at low weight fractions. The onset velocity of air entrainment exhibited a peak even at concentration-independent low viscosity regimes at low weight fractions < 0.1 wt %. The peak velocity was obtained at a higher particle weight fraction as the particle diameter increases.

where v_{ae} and v_{ae0} are the onset velocities in the suspension and the filler-free fluid, respectively. It was found from Figure 4 that the onset velocity of air entrainment first increases and then decreases with increasing particle diameter. The onset velocity reaches a peak at the specific particle diameter of 30 μm. The resultant maximum velocity at the peak was found to be $(v_{ae} - v_{ae0})/v_{ae0} = 0.91$, indicating that the suspension was successfully applied onto the moving surface at a speed as much as twice that of the filler-free liquid.

In the second series of experiments, the particle weight fraction was varied, while the particle diameter was kept constant. Figure 5 shows the onset velocity of air entrainment and bulk suspension viscosity for different particle weight fractions. The measured suspension viscosity (μ) agreed with that of the filler-free liquid (μ_0) at low weight fractions less than 0.1 wt % (Figure 5a). At higher weight fractions, the viscosity monotonically increased with increasing particle weight fractions. The independence of viscosity from the particle diameter is consistent with the classical hydrodynamic theories based on simple solid–liquid interactions. On the contrary, the onset velocity of air entrainment exhibited a peak even at concentration-independent low-viscosity regimes of $C_p \leq 0.1\%$. The peak velocities were obtained at higher particle weight fractions as the particle diameter increased. Once the empirical power law holds, an increase in viscosity should lead to a decrease in the onset velocity of air entrainment. However, Figure 5b revealed a significant increase in onset velocity up to $(v_{ae} - v_{ae0})/v_{ae0} = 0.5$ at particle concentrations of $C_p = 1$ wt %. These results provide conclusive evidence that the dynamic wetting failure in suspensions cannot simply be explained by

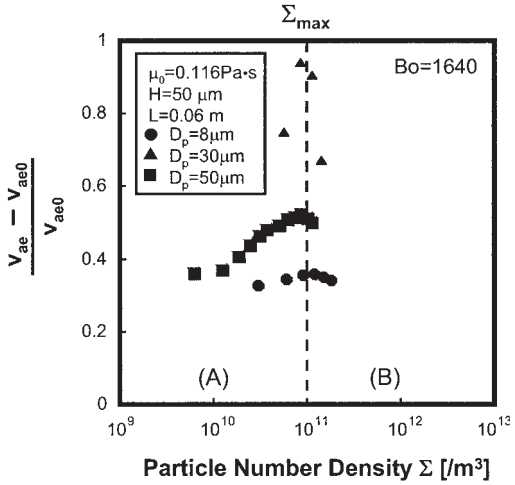

Figure 6. Variation in onset velocity of air entrainment with particle number density.

The onset velocity of air entrainment exhibits a peak at the same particle number density of $\Sigma_{max} = 1 \times 10^{11}/m^3$, independent of particle diameter.

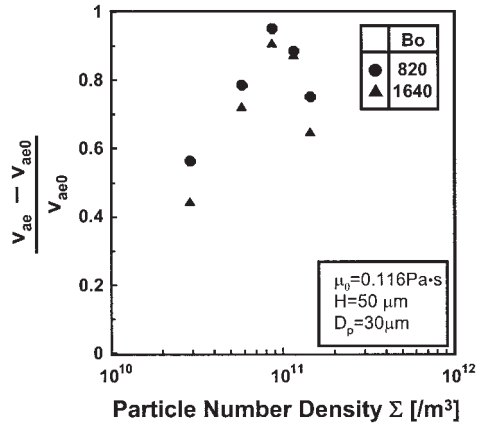

Figure 7. Effect of Bond number on onset velocity of air entrainment.

The onset velocity of air entrainment exhibits a peak at the same critical number density of $\Sigma = \Sigma_{max}$ for any Bond number. The viscosity and the surface tension of the liquid medium were $\mu_0 = 0.116$ Pa·s and $\sigma = 0.0209$ N/m.

the variation in bulk liquid viscosity. In contrast to filler-free fluids, the suspension does not obey the power law.

To understand how the fillers interact to postpone the onset of air entrainment, we replotted the measured onset velocity of air entrainment against the particle number density, that is, the number of particles per unit liquid volume. As shown in Figure 6, the onset velocity of air entrainment was found to exhibit a peak at the same particle number density of $\Sigma_{max} = 1 \times 10^{11}/m^3$, which was independent of particle diameter. The existence of such a critical number density strongly suggests that the air entrainment in the suspension is no longer considered a bulk phenomenon but rather involves interfacial contributions of each filler component. Figure 6 also reveals that the suspension exhibits two distinct flow regimes with increasing particle number density, that is, the onset velocity of air entrainment increases at low number densities of $\Sigma < \Sigma_{max}$ (Regime A), whereas it decreases at high number densities of $\Sigma > \Sigma_{max}$ (Regime B).

The gravitational or inertial force acting on the liquid is also known to postpone the onset of air entrainment because it pressurizes the meniscus onto the solid to stabilize the contact lines.[12,13] To evaluate the effect of gravitational force on the critical number density, we performed velocity measurements at different liquid heights in the die ranging from $L = 0.03$ to $L = 0.06$ m. The resultant Bond number, $Bo = \rho g L^2/\sigma$, the ratio of the gravitational force to the surface tension force, ranged between 800 and 1700. The measured onset velocity of air entrainment monotonically increased with increasing Bond number because of the higher static liquid pressure. However, the normalized onset velocity exhibits a peak at the same critical number density of $\Sigma = \Sigma_{max}$ for any Bond number, as shown in Figure 7, suggesting that the critical particle number density is a unique physical factor that does not depend on either gravitational or surface tension forces.

The peculiar air entrainment features can be understood by considering a particle motion that splits the intruding air into smaller segments. The possible air–film-splitting sequence is schematically shown in Figure 8. Consider a flowing particle that invades the air film and contacts the moving surface against the lubrication pressure (Figure 8a). Because the contact motion accelerates the particle to the surface velocity, the resulting strong shear stress around the particle is responsible for splitting the air film into fingers. The air finger subsequently shrinks as a result of the high capillary pressure at the curved finger tip (Figure 8b). For the case of low particle number densities, only a few neighboring particles can contact the surface, and thus the film splits into relatively thick fingers. The fast pressure-driven flow in the thick finger cancels the drag

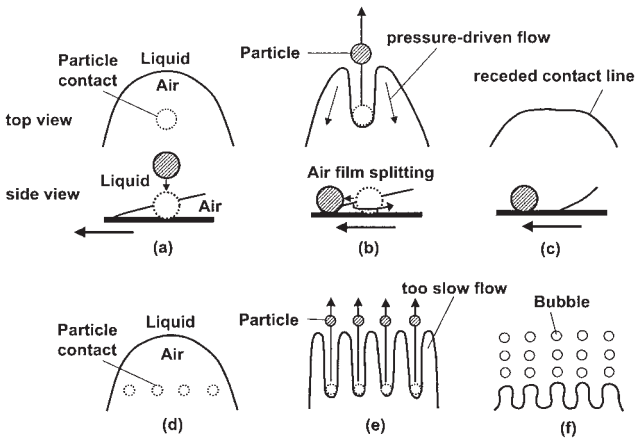

Figure 8. Two film-splitting sequences at low and high particle number densities.

(a) Particle invades the air film and contacts the moving surface against the lubrication pressure. (b) The shear stress around the particle splits the air film into fingers that subsequently shrink as a result of the adverse pressure gradient. (c) The pressure-drive flow cancels the drag flow, pulls the finger further upstream, and restabilizes the contact line. For high particle number densities, (d) more than one particle can instantly contact the surface to form thinner air fingers. (e) The thinner fingers involve slower pressure-driven flow, which no longer competes the drag flow. (f) The air fingers break up into small bubbles because of growing interfacial instability.

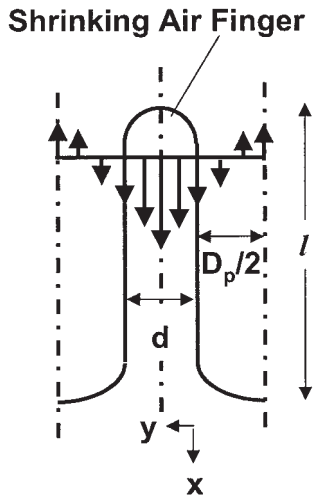

Figure 9. Unidirectional lubrication flows in an air finger and liquid threads.

A circular finger edge creates the adverse pressure gradient. The width of the air finger d equals the mean separation length between contacting particles.

flow, pulls the finger further upstream, and eventually causes the dynamic contact line to recede at even higher surface speeds (Figure 8c). On the contrary, more than one particle can instantly contact the surface for higher particle number densities (Figure 8d). The resulting thinner air finger involves a pressure-driven flow that is too slow to compete against the drag flow (Figure 8e). Thus the fingers no longer shrink but rather break up into fine bubbles as a result of the growing interfacial instability (Figure 8f), leading to an onset of dynamic wetting failure at lower surface speeds. This physical picture is consistent with the increase and decrease in onset velocity of air entrainment with increasing particle number density (see Regimes A and B in Figure 6).

Lubrication Theory

To support the proposed mechanism, we applied a one-dimensional lubrication theory for describing a sequential series of particle contacts and film splittings. For simplicity, consider a two-dimensional air finger with a constant thickness and a length l as shown in Figure 9. The x-component of the Navier–Stokes equation in the air finger was reduced to $\partial p/\partial x = \mu_A \partial^2 u/\partial y^2$ and the y-component to $\partial p/\partial y = 0$, where p is the local air pressure, u is the air velocity in the x-direction, and μ_A is the air viscosity. Assuming a circular finger edge, the pressure gradient in the x-direction equals the capillary pressure difference $-2\sigma/(dl)$, where σ is the surface tension. Substituting the pressure gradient and integrating the parabolic velocity profile in the y-direction yield the mean air velocity in the finger as $u_m = u_i + \sigma d/(6\mu_A l)$, where u_i denotes the velocity component at the interface between the air finger and the remaining liquid thread. The local stress balance at the interface gives the interfacial velocity as $u_i = \sigma D_p/(6\mu_0 l)$. Thus the mean shrinkage velocity of the air finger is expressed in terms of the ratios of viscosities and length scales as

$$u_m = \frac{\sigma d}{6\mu_A l}\left[1 + \left(\frac{D_p}{d}\right)\left(\frac{\mu_A}{\mu_0}\right)\right] \tag{1}$$

The time required for the finger shrinkage (τ_s) and the time interval of particle contact (τ_c) are the key physical factors for describing the postponed air entrainment in suspensions. Considering an air finger shrinking with a mean velocity of u_m, the shrinkage timescale is given by $\tau_s = l/u_m$. Substituting Eq. 1 into the expression yields

$$\tau_s = 6\mu_A l^2/(\sigma d) \tag{2}$$

where the second term on the right side of Eq. 1 is neglected because the liquid viscosity of interest is much higher than the air viscosity, given that $\mu_A/\mu_0 \ll 1$.

We assume that particles are homogeneously suspended with a mean separation length d. The contact time interval is simply expressed as

$$\tau_c = d/v_{ae0} \tag{3}$$

where v_{ae0} is the onset velocity of air entrainment in the filler-free fluid. The characteristic velocity is assumed to be given by v_{ae0} in this time interval because the particles before contact play no role in the increase in onset velocity of air entrainment.

Here we note that the two timescales exhibit an opposite dependency on the particle number density. Because the particle separation length is simply expressed as $d = \Sigma^{-1/3}$ in a homogeneous suspension, τ_s and τ_c in Eqs. 2 and 3 become increasing and decreasing functions with respect to the particle number density. In the case of a low particle number density, the contact time interval becomes much longer than the time required for the finger shrinkage ($\tau_c \gg \tau_s$), and thus the finger can completely shrink before the following particle comes into contact with the surface. At high particle number densities, on the contrary, the finger does not shrink during a finite contact interval ($\tau_c \ll \tau_s$).

The two relevant timescales allow us to estimate the postponed onset velocity of air entrainment in suspensions. We assume that the onset velocity remains v_{ae0} in the time interval of τ_c, whereas it increases to $v_{ae0} + u_m$ in the time interval of τ_s, that is, a higher finger shrinkage velocity restabilizes the contact line to a higher speed. Assuming the sequential particle contact and the finger shrinkage, the time-averaged onset velocity is given by

$$v_{ae} = \frac{\tau_c v_{ae0} + \tau_s(v_{ae0} + u_m)}{\tau_c + \tau_s} \tag{4}$$

Substituting Eqs. 2 and 3 into Eq. 4 and setting $d = \Sigma^{-1/3}$ yield the expression for the normalized onset velocity of air entrainment as

$$\frac{v_{ae} - v_{ae0}}{v_{ae0}} = \frac{1}{\left(\dfrac{1}{\Sigma^{1/3} l} + 6\Sigma^{1/3}\mathrm{Ca}\, l\right)} \tag{5}$$

where the capillary number in the air is defined as $\mathrm{Ca} = \mu_A v_{ae0}/\sigma$. It is immediately clear from Eq. 5 that the increase in onset velocity is proportional to $\Sigma^{1/3}$ at low particle number

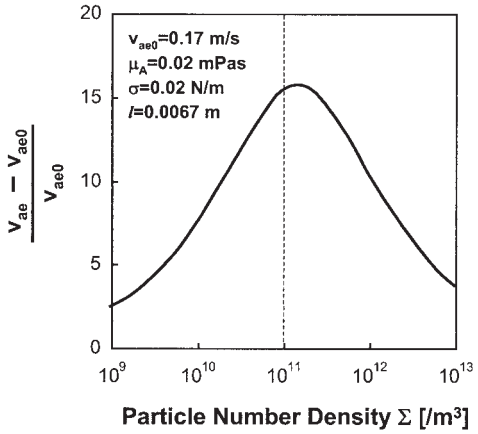

Figure 10. An example of the onset velocity of air entrainment calculated from the lubrication theory.

The increase and decrease in onset velocity with increasing particle number density are consistent with experiments shown in Figure 6.

densities, whereas it obeys $(v_{ae} - v_{ae0})/v_{ae0} \propto \Sigma^{-1/3}$ at high number densities. Figure 10 shows an example of the onset velocity calculated from Eq. 5. The increase and decrease in onset velocity of air entrainment with increasing particle number density are consistent with the experimental results shown in Figures 6 and 7.

To verify the lubrication model in detail, the solution of $dv_{ae}/d\Sigma = 0$ was obtained to evaluate the critical particle number density at which the onset velocity of air entrainment exhibits a peak. The solution gives

$$\Sigma_{\max} = \frac{1}{(6\,\mathrm{Ca})^{3/2} l^3} \tag{6}$$

Equation 6 shows that the critical number density does not depend on either particle diameter or Bond number. This is consistent with the experimental results shown in Figures 6 and 7. Furthermore, substituting typical experimental values of $\mu_A = 2 \times 10^{-5}$ Pa·s, $v_{ae0} = 0.176$ m/s, $\sigma = 0.02$ N/m, and $l = 6.6 \times 10^{-3}$ m into Eq. 6 yields the capillary number of $\mathrm{Ca} = 1.76 \times 10^{-4}$ and the critical density of $\Sigma_{\max} = 1 \times 10^{11}/\mathrm{m}^3$, showing good agreement with the measured critical number density shown in Figure 6.

The expression for the critical number density also shows that the onset velocity of air entrainment reaches a peak at a critical particle diameter. Transforming the particle number density in Eq. 6 to the particle weight fraction C_p, we obtain the critical particle diameter at a peak as

$$D_{p,\max} = 4.45\sqrt{\mathrm{Ca}}\left(\frac{\rho C_p}{\pi \rho_p}\right)^{1/3} l \tag{7}$$

where ρ and ρ_p are the densities of the liquid and the particle, respectively. The substitution of $\mathrm{Ca} = 1.76 \times 10^{-4}$, $C_p = 0.1$ wt %, $\rho = 975$ kg/m^3, $\rho_p = 1200$ kg/m^3, and $l = 6.6 \times 10^{-3}$ m into Eq. 7 gives the particle diameter of $D_{p,\max} = 25$ μm, showing good agreement with the experiments shown in Figure 4. These facts provide unambiguous evidence that the postponement of air entrainment in suspensions can be explained by considering the dynamic interplay between the viscous drag flow and the competing pressure-driven flow in the split air finger.

From a practical perspective, it is desirable to postpone the onset of air entrainment to a higher speed because an air bubble is detrimental to the quality of the final coating product. Substituting Eq. 6 into Eq. 5 gives the maximum onset velocity expressed in terms of the capillary number in the gas phase as

$$\left(\frac{v_{ae} - v_{ae0}}{v_{ae0}}\right)_{\max} = \frac{\mathrm{Ca}^{-1/2}}{2\sqrt{6}} \tag{8}$$

Substitution of the capillary number of $\mathrm{Ca} = 1.76 \times 10^{-4}$ into Eq. 8 gives the maximum onset velocity of 14, implying that air entrainment in the suspension can be postponed to a speed one order of magnitude faster than that in the filler-free fluid. Because the experimental observation showed an onset velocity of less than unity (see Figures 4 and 5), the maximum onset velocity predicted from the simplest lubrication theory is not satisfactory in a quantitative sense. Furthermore, the maximum onset velocity in Eq. 8 is independent of particle diameter, whereas the measured maximum velocity shows a strong dependency on particle diameter even at the same capillary number (see Figure 6). Nevertheless, our lubrication model provides a start toward a basic understanding of how the introduction of fillers delays the onset of dynamic wetting failure in suspension coatings.

One might argue that the postponed air entrainment in suspensions seems to be similar to that observed on a *rough* surface. Indeed, a properly chosen surface roughness is known to successfully postpone the dynamic wetting failure above a critical liquid viscosity.[14,15] This feature is attributed to the contact line motion that does not wet the surface along the peak and the valley but rather skips from peak to peak. For filler-free fluids on a rough surface, the onset velocity of air entrainment increases with increasing liquid viscosity because more liquid can skip the peaks. In the present experiment, however, an increase in silicone oil viscosity μ_0 from 0.0538 to 0.312 Pa·s led to a monotonic decrease in the normalized onset velocity $(v_{ae} - v_{ae0})/v_{ae0}$ from 0.82 to 0.33, showing a reverse viscosity dependency from the roughness effect. The peculiar dependency of onset velocity on liquid viscosity is one of the unique characteristics of the filler-induced air entrainment. Based on our film-splitting concept, the volume occupied by a contacting particle is replaced by the liquid to form a liquid thread between the air fingers. If the liquid viscosity is too high to compensate for the particle volume in a finite time, the "void" is readily filled with the surrounding air, and thus no air finger forms. This is possibly the reason that the higher liquid viscosity induces a lower increase in the onset velocity of air entrainment in suspension coatings.

Conclusions

We experimentally demonstrated that the onset of air entrainment is significantly postponed in suspensions of spherical solid particles. The maximum onset velocity was obtained at a specific particle number density that does not depend on either the particle diameter or the Bond number. In contrast to the

dynamic wetting failure in filler-free fluids, the instability through a free-surface cusp in the suspension is no longer considered a bulk phenomenon but rather involves interfacial contributions of each filler component. The unusual air entrainment behavior was characterized by newly considering a forced air-film splitting arising from the particle invasion against the lubrication pressure. The one-dimensional lubrication model provides good explanations for the observed dependencies of the air entrainment velocity on the particle number density. However, the maximum onset velocity predicted from the simple model is much higher than the measurements, suggesting that the present model is not satisfactory in a quantitative sense. We need further studies to clarify the detailed physical mechanism of the air entrainment by taking into account the three-dimensional interfacial instability coupled with the microscopic flows around each particle.

Acknowledgments

This work was supported in part by the Grant-in-Aid (No. 14750608) for Encouragement of Young Scientists from the Japan Society for the Promotion of Science and the Industrial Technology Research Grant Program from New Energy and Industrial Technology Development Organization of Japan. We gratefully acknowledge the continuing encouragement of Dr. Kitaro Adachi.

Literature Cited

1. Mues W, Hens J, Boiy L. Observation of a dynamic wetting process using laser-Doppler velocimetry. *AIChE J*. 1989;35:1521-1526.
2. Miyamoto K. On the mechanism of air-entrainment. *Ind Coat Res*. 1991;1:71-88.
3. Blake TD, Ruschak KJ. A maximum speed of wetting. *Nature*. 1979; 282:489-491.
4. Burley R, Kennedy BS. An experimental study of air entrainment at a solid/liquid/gas interface. *Chem Eng Sci*. 1976;31:901-911.
5. Eggers J. Air entrainment through free-surface cusps. *Phys Rev Lett*. 2001;86:4290-4293.
6. Simpkins PG, Kuck VJ. On air entrainment in coatings. *J Colloid Interface Sci*. 2003;263:562-571.
7. Teletzke GF, Davis HT, Scriven LE. Wetting hydrodynamics. *Rev Phys Appl*. 1988;23:989-1007.
8. Benkreira H, Cohu O. Angling the wetting line retards air entrainment in premetered coating flows. *AIChE J*. 1998;44:1207-1209.
9. Cohu O, Benkreira H. Air entrainment in angled dip coating. *Chem Eng Sci*. 1998;53:533-540.
10. de Ruijter MJ, Blake TD, de Coninck J. Dynamic wetting studies by molecular modelling simulations of droplet spreading. *Langmuir*. 1999;15:7836-7847.
11. Gutoff EB, Kendrick CE. Dynamic contact angles. *AIChE J*. 1982;28: 459-466.
12. Blake TD, Clarke A, Ruschak KJ. Hydrodynamic assist of dynamic wetting. *AIChE J*. 1994;40:229-242.
13. Yamamura M, Suematsu S, Kajiwara T, Adachi K. Experimental investigation of air entrainment in a vertical liquid jet flowing down onto a rotating roll. *Chem Eng Sci*. 2000;55:931-942.
14. Clarke A. Coating on a rough surface. *AIChE J*. 2002;48:2149-2156.
15. Benkreira H. The effect of substrate roughness on air entrainment in dip coating. *Chem Eng Sci*. 2004;59:2745-2751.

Manuscript received Aug. 18, 2004, and revision received Jan. 4, 2005.